catalysts

MDPI

Article

Photocatalytic Reduction of Nitrates and Combined Photodegradation with Ammonium

Francesco Conte [1], Veronica Pellegatta [1], Alessandro Di Michele [2], Gianguido Ramis [3] and Ilenia Rossetti [1,*]

[1] Chemical Plants and Industrial Chemistry Group, Dip. Chimica, Università degli Studi di Milano, CNR-SCITEC and INSTM Unit Milano-Università, Via C. Golgi 19, 20133 Milan, Italy; francesco.conte@unimi.it (F.C.); veronica.pellegatta@libero.it (V.P.)
[2] Physics and Geology Department, Università di Perugia, Via Pascoli, 06123 Perugia, Italy; alessandro.dimichele@unipg.it
[3] Dip. Ing. Chimica, Civile ed Ambientale, Università degli Studi di Genova and INSTM Unit Genova, Via all'Opera Pia 15A, 16145 Genoa, Italy; gianguidoramis@unige.it
* Correspondence: ilenia.rossetti@unimi.it

Abstract: Bare titania and metal-promoted TiO_2 catalysts were employed in the treatment of nitrates, which are ubiquitous pollutants of wastewater. The results show that the process can be carried out under visible light (from a white light LED lamp) and, in the best case, 23.5% conversion of nitrate was obtained over 4 h with full selectivity towards N_2 by employing 0.1 mol% Ag/TiO_2 prepared by flame spray pyrolysis. Moreover, the performance was worse when testing the same catalysts with tap water (11.3% conversion), due to the more complex composition of the matrix. Finally, it was found that photoreduction of nitrate can be effectively performed in combination with photo-oxidation of ammonium without loss in the activity, opening up the possibility of treating highly polluted wastewater with a single process. The latter treatment employs the two contaminants simultaneously as electron and holes scavengers, with very good selectivity, in a completely new process that we may call Photo-Selective Catalytic Reduction (Photo-SCR).

Keywords: wastewater treatment; nitrogen-containing pollutants; nitrate photoreduction; SCR; photocatalysis; titania

Citation: Conte, F.; Pellegatta, V.; Di Michele, A.; Ramis, G.; Rossetti, I. Photocatalytic Reduction of Nitrates and Combined Photodegradation with Ammonium. *Catalysts* **2022**, *12*, 321. https://doi.org/10.3390/catal12030321

Academic Editor: Detlef W. Bahnemann

Received: 23 January 2022
Accepted: 4 March 2022
Published: 11 March 2022

1. Introduction

Nitrogen mainly occurs in the form of inert diatomic molecules, which can be converted into more reactive compounds through the biological nitrogen fixation cycle. However, since the development of the Haber–Bosch process, we faced a massive production of substances that contain activated nitrogen such as ammonia and nitrates, which are commodities widely used in fertiliser formulation. These compounds have a huge impact on the cycle of nitrogen since the net conversion of N_2 from the atmosphere is multiplied almost four-fold, with respect to the amount naturally fixed by plants [1]. Moreover, traditional agriculture techniques are not efficient in employing fertiliser, which is easily dispersed into the atmosphere, and where inorganic nitrogen contributes to rain acidification and to NO_x formation [2]. Fertiliser can also leach from the soil due to rain and irrigation systems, subsequently entering the water cycle from the groundwater where nitrogen-containing compounds cause eutrophication and pollution due to their intrinsic toxicity to living organisms [3]. Furthermore, groundwater is one of the primary sources of drinking water, but the World Health Organisation (WHO) defines it "drinkable" only if it does not contain more than 50 ppm (parts per million) of NO_3^- and 3 ppm of NO_2^-, whereas the ammonia must not exceed 500 ppb (parts per billion) [4]. Although these are critical thresholds, noxious effects have been observed even at lower concentrations, especially for the smallest fish and microorganisms [5], while for humans, the daily usage of polluted water can lead to irritations, DNA damage, tumoral formation and disequilibria in body pH [6,7].

Thus, when the pollutant concentration is higher than the value tolerated by the environment, it is necessary to treat the water source. For instance, contaminated water can be cleaned via biological denitrification, which is a safe process and effective in most cases. However, it requires to constantly feed the microorganisms with a suitable carbon source that is exploited by the latter to perform the reduction of nitrate to molecular nitrogen [8]. Furthermore, alternatives processes are ion-exchange chromatography, which can treat highly polluted streams but essentially creates a more concentrated solution of which to dispose, or finer approaches such as ultrafiltration, reverse osmosis and electro-dialysis, for which the cost of disposal is increased significantly [9,10].

We explore here an innovative photocatalytic approach which exploits appropriate semiconductors to absorb light and promote RedOx reactions through photogenerated holes and electrons. In detail, titanium dioxide is a widely employed material (safe, inexpensive and stable) and a well-known photocatalyst that absorbs in the ultraviolet region due its wide band gap, and which depends on its polymorphic structure (3.0 eV for the rutile phase and 3.2 eV for anatase) [11–13]. Moreover, in form of nanoparticles, it has been used to promote several reactions such as degradation of organic pollutants, CO_2 activation, wastewater treatment and water splitting to produce hydrogen [14–16]. Anyway, as a photocatalyst, it is limited by its wide band gap and by the fast recombination between the photogenerated electrons and holes. To improve both aspects the properties of the catalyst can be tuned by deposition of metal co-catalysts over its surface, for instance Cu, Ag, Au, Pt: it is an established method to extend the lifetime of the photogenerated charges and to narrow the band gap, for instance thanks to the reduction treatment of the photocatalyst or for plasmonic surface resonance, thus allowing to operate under visible light [17]. This latter effect may be exploited through different effects. Some metals contribute to light absorption thanks to their own plasmonic resonance (e.g., Au). In other cases, the incorporation of the metal in the structure of the semiconductor can lead to doping. Finally, most of the exemplified metals are well known reduction catalysts, promoting the effective reduction of TiO_2 which is a well-known method to decrease titania band gap [18–20].

Furthermore, the band energies of titania, whose potential is −0.05 V for the conduction band and 2.7 V for the valence one, makes it a strong oxidising agent and a mild reducing one [21] and, in addition, they are suitable to perform either the photo-reduction of nitrite and nitrate or ammonium photo-oxidation, as the standard potential of the N_2/NH_3 couple is ca. 0.06 V, whereas for the couples NO_3^-/N_2 and NO_2^-/N_2 it is 1.25 V and 1.52 V, respectively.

In this study, we evaluated the photocatalytic activity of several titania-based catalysts that were obtained either from commercial titania or homemade TiO_2 (prepared by flame spray pyrolysis, FSP) and promoted variously via the addition of metal co-catalysts. FSP-prepared materials were applied for this reaction and proved effective. These materials were employed in the treatment of water solutions containing sodium nitrate at selected pH values, in the attempt to simulate wastewater composition, and the process was carried out under UV or visible light irradiation after optimisation of the reaction parameters, with the aim of obtaining an efficient and sustainable way to degrade a pollutant which can compete with well-established water treatment techniques. The simultaneous abatement of ammonia and nitrates was also explored as a fully new process, here called Photo-Selective Catalytic Reduction (Photo-SCR). The latter approach is an advancement for the one-step abatement of two noxious pollutants simultaneously and has not been presented in detail in the open literature.

2. Results and Discussion

2.1. Material Characterisation

Nitrogen adsorption and desorption isotherms were used to estimate the specific surface area and the pore volume of the catalysts (Figure 1). As reported in Table 1, the deposition of a co-catalyst generally caused an increase in the surface area and in the pore volume of these materials, although the gains depend on the metal deposited and the

temperature at which the reduction was performed after impregnation, the minimum effect being observed with Au. This is ascribed to the formation of agglomerates of particles inducing interparticle porosity (meso- and macro-), scarcely present in the bare material, and constituted by dense nanoparticles poorly agglomerated. In addition, the catalysts supported on FSP titania showed a higher surface area due to the smaller size of the particles compared to those of P25. Moreover, the micropore pore volume of the metal-promoted catalysts was generally lower than the commercial benchmark (P25) and this is likely to be caused by pore blockage by the metal and a collapsing of the micropores that occurs during the reduction at high temperature.

Table 1. Results of the characterisation analysis of selected catalysts.

	P25					FSP			
Sample	**-**	**0.1% Pt**	**0.1% Ag**	**0.1% Au**	**1% Ag**	**-**	**0.1% Pt**	**0.1% Ag**	**0.1% Au**
Phase %	A(78) + R(22)	A(87) + R(13)	A(87) + R(13)	A(87) + R(13)	/	A(65) + R(35)	A(71) + R(29)	A(70) + R(30)	A(70) + R(30)
BET surface Area (m^2/g)	45	55	61	47	57	68	59	72	65
Crystallite size (nm)	15	21	21	21	/	24	26	30	28
Total pore volume (cm^3/g)	0.11	0.32	0.21	0.38	0.54	0.14	0.25	0.36	0.30
t-plot micropore volume (cm^3/g)	0.012	0.0036	0.0040	0.0026	0.0052	0.02	0.0037	0.00044	0.0003
BJH adsorption pore width (nm)	22	23	24	25	36	20	19	17	16
Band gap (eV)	3.41	3.12	3.23	3.27	3.15	3.23	3.10	3.24	3.11

Figure 2 illustrates the XRD patterns of selected materials. The latter shows two titania phases, anatase and rutile, with the anatase accounting for 70–87% of the whole structure. The content of anatase was generally lower for the FSP samples due to a possibly higher temperature of the flame during synthesis or to a longer residence time in the hottest part of the flame. Regardless, the graph shows a small variation for those peaks associated with the main phases, thus the presence of a co-catalyst does not influence its phase composition. In addition, there is no evidence of new peaks, or other phases, due to metal deposition. This is in line with the very low metal loading and its high dispersion. The increase in the anatase/rutile ratio upon metal addition and reduction may be better explained considering the partial reduction of TiO_2. The transition from anatase to rutile is favourable over the whole temperature range but becomes significant (at ambient pressure) only above ca. 600 °C, with kinetics depending on many factors [22]. The oxygen defectivity forming upon partial reduction of titania (black or grey titania) can also alter the ratio between the two main phases depending on the way reduction is achieved. A possible increase in the anatase/rutile ratio even after annealing at high temperature has been reported [23].

DR-UV-Vis analysis was performed in order to calculate the band gap (BG) of the active materials. The raw data were elaborated according to the Tauc plot method, corrected where necessary to take into account overlapping contributions, as suggested elsewhere [24]. From Table 1, it is evident that the addition of a co-catalyst was effective in reducing the BG of the bare titania, which is about 3.41 eV; in the case of FSP titania with 0.1% of Au, its value dropped to 3.11 eV, thus improving the absorption of visible light. This band gap reduction is here attributed to the reduction of the metallic co-catalysts at high temperature, which causes a partial reduction of the titania which is better catalysed by the presence of the metal itself.

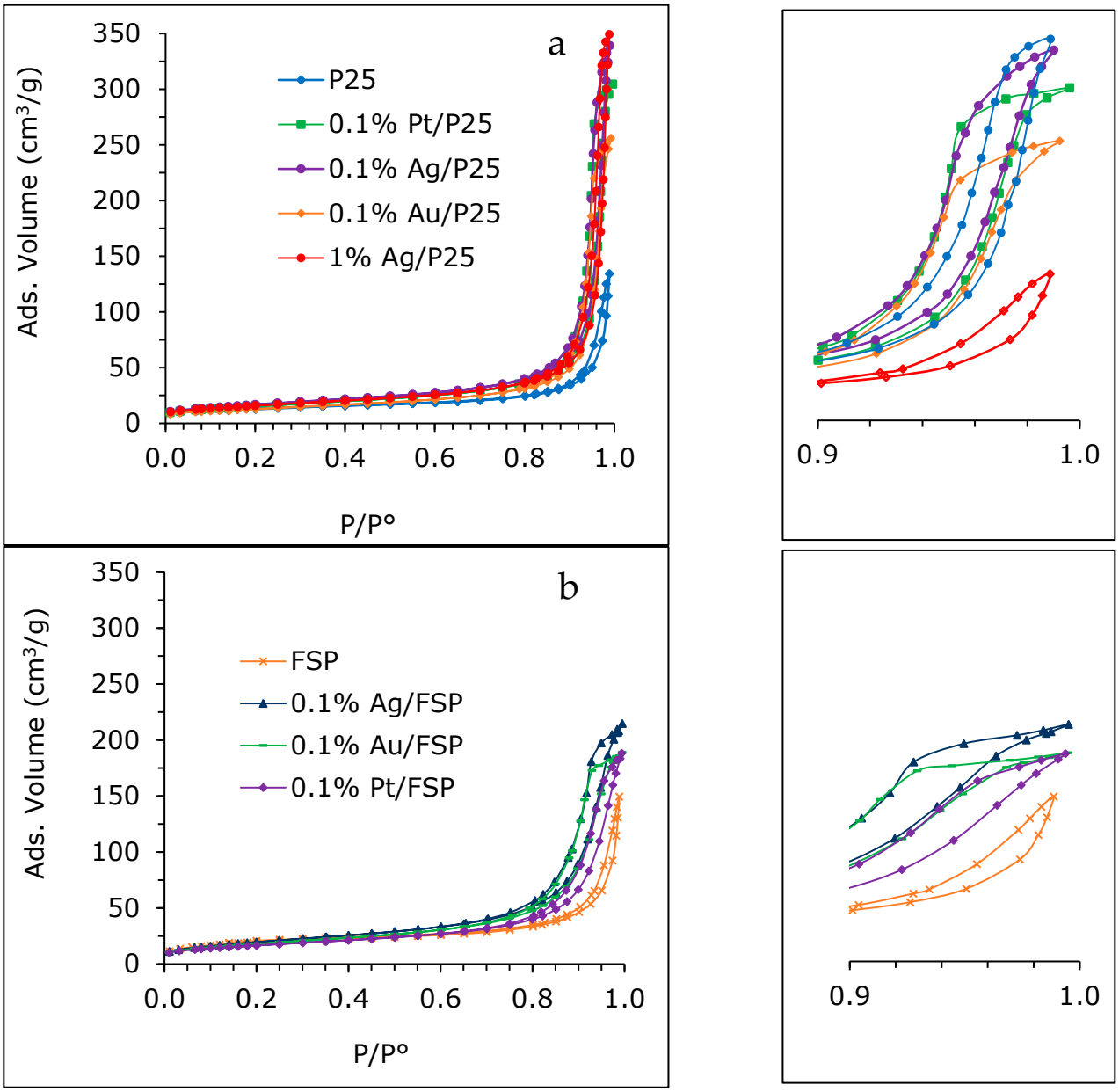

Figure 1. BET adsorption-desorption isotherms of selected catalysts. Adapted from [25]. (**a**) Samples supported on P25 Titania; (**b**) samples supported on FSP Titania.

Morphologic analysis by SEM shows very uniform particle size (15–25 nm) for P25 and slightly smaller particles for FSP samples, even when accompanied by larger spheres, sometimes hollow, as sporadically detected by TEM microscopy (Figure 3). Metal loading did not affect the morphology, even after high thermal treatment, thanks to both synthesis methods, using high temperature flames, which impart high thermal resistance to the material. TEM analysis also revealed a quite uniform distribution of the metal over the titania particles, confirmed by SEM–EDX mapping. EDX also confirmed the average metal loading.

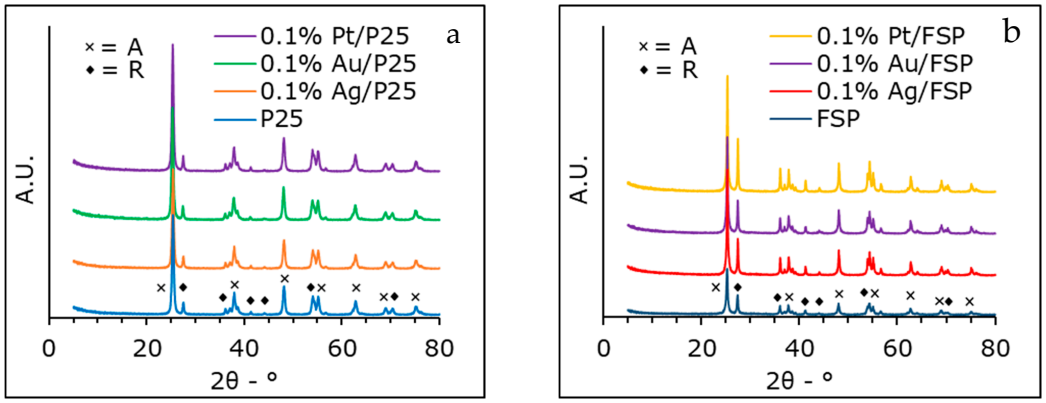

Figure 2. XRD characterisation results for selected catalysts. The peaks labelled with the cross belong to anatase, while the rhombus highlights the peaks of rutile phase. (**a**) Samples supported on P25 Titania; (**b**) samples supported on FSP Titania.

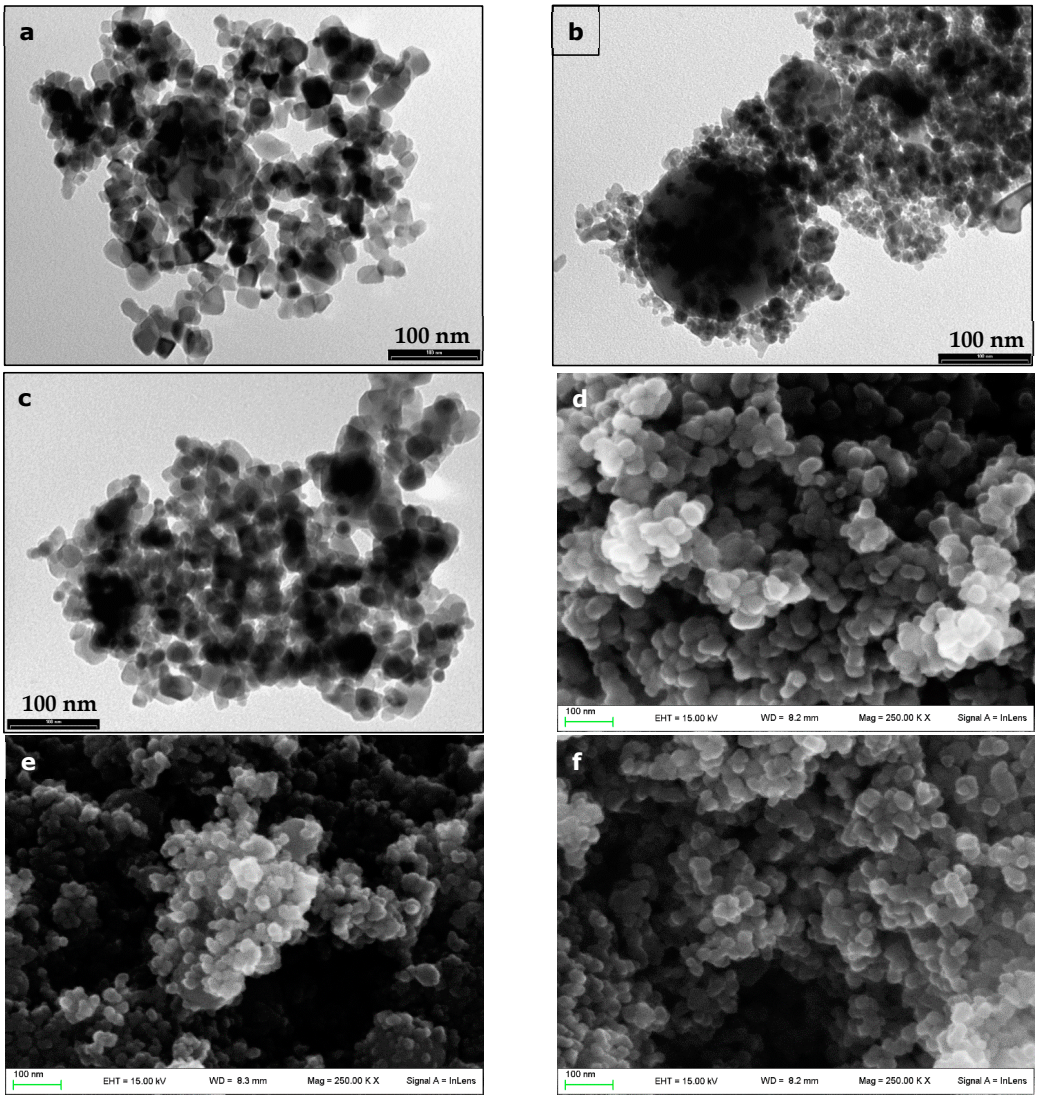

Figure 3. TEM micrographs of (**a**) 1% Ag/P25, (**b**) 0.1% Ag/FSP, (**c**) 0.1% Au/P25 and SEM pictures of (**d**) 1% Ag/P25, (**e**) 0.1% Ag/FSP, (**f**) 0.1% Au/P25.

2.2. Photo-Reduction of Nitrate Promoted under UV Light Irradiation

Blank tests were carried out by adding the catalyst with no irradiation and by irradiating the solution without a catalyst. In both cases no significant change of the reactant concentration was observed.

Nitrate photo-reduction is a multistep process that involves the reaction of that species, adsorbed over the photo-catalyst surface, with the photo-generated electrons. Nitrite is the first intermediate obtained (Reaction 1); this substrate is then subject to further reduction to molecular nitrogen (Reaction 2). It is crucial to work with conditions that prevent the overreduction of nitrate/nitrite to ammonia (Reaction 3), since that path simply converts one pollutant into another.

$$NO_3^- + 2e^- + 2H^+ \rightarrow NO_2^- + H_2O \quad (1)$$

$$2NO_2^- + 6e^- + 4H^+ \rightarrow N_2 + 2H_2O \quad (2)$$

$$NO_2^- + 6e^- + 8H^+ \rightarrow NH_4^+ + 2H_2O \quad (3)$$

The very first tests were carried out with the reactor in a sealed configuration, using 0.1% Pt/FSP as the active material, due to its good performance achieved in previous experiments [15], using an UV lamp as the photon source. Based on the results of previous work [26], we decided to operate the treatment at pH 5, since slightly acidic values increased both the conversion of nitrate and the selectivity towards N_2. The solution was kept under irradiation for 24 h in order to follow the time evolution of the reaction.

As reported in Figure 4, the conversion of the nitrate was moderate and did not exceed 25% after 24 h of irradiation. Some ammonium was detected among the products, as the result of an overreduction [27]. Furthermore, looking at the trend of nitrogen evolution, it seems that the catalyst is not so active in the early stage of the treatment, at least towards our target product, since appreciable amounts of N_2 were detected only after 5 h of exposure. Overall, we measured a negligible selectivity towards NO_2^-.

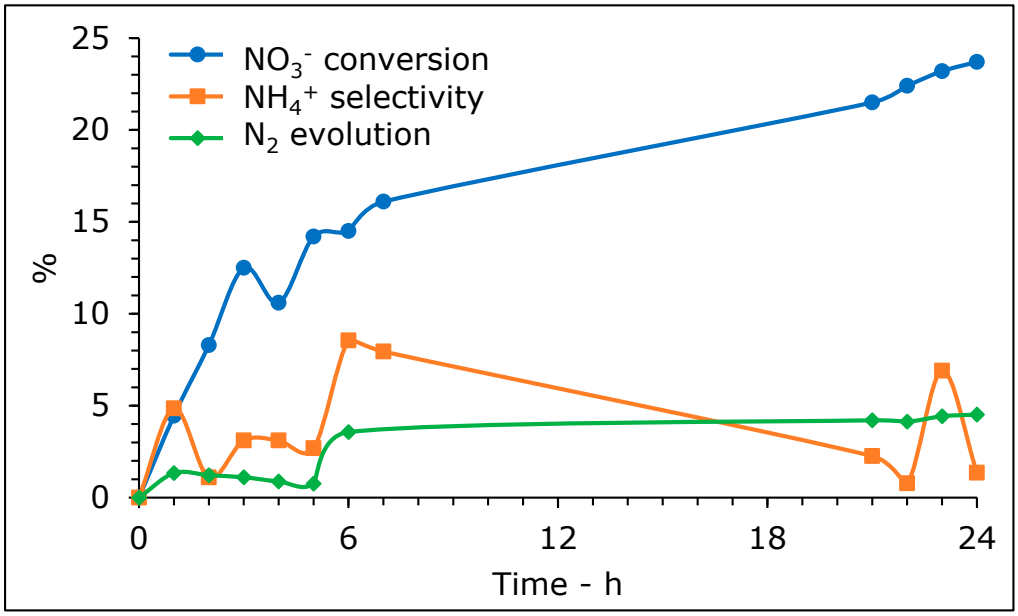

Figure 4. Photo-reduction of NO_3^- under UV irradiation (Irradiance = 260 W/m^2) with 0.1% Pt/FSP as photocatalyst (1 g/L), $NaNO_3$ (6 mM), pH 5, rt and 250 mL of solution (Reactor 1).

2.3. Photo-Reduction under Visible Light (LED)

The first parameter to be tuned was the concentration of the pollutant. We preferred to work with reactor 2, since measuring very low amounts of contaminant could significantly

increase the experimental error. In addition, 0.1% Ag/FSP catalyst was employed, already used in the case of UV treatment [15], due to its low band gap which allows light absorption in the visible range.

As illustrated in Figure 5, the best results were obtained with a nitrate concentration of 1.7 mM, with a 23.5% conversion at the end of the treatment, which is an impressive result considering the low power of the LED lamp (about 30 W) and that the incident photons have much less energy than the those emitted by the UV lamp. Nevertheless, the deposition of reduced noble metals over the titania surface is well known to increase the harvesting of visible light by a photocatalyst [28].

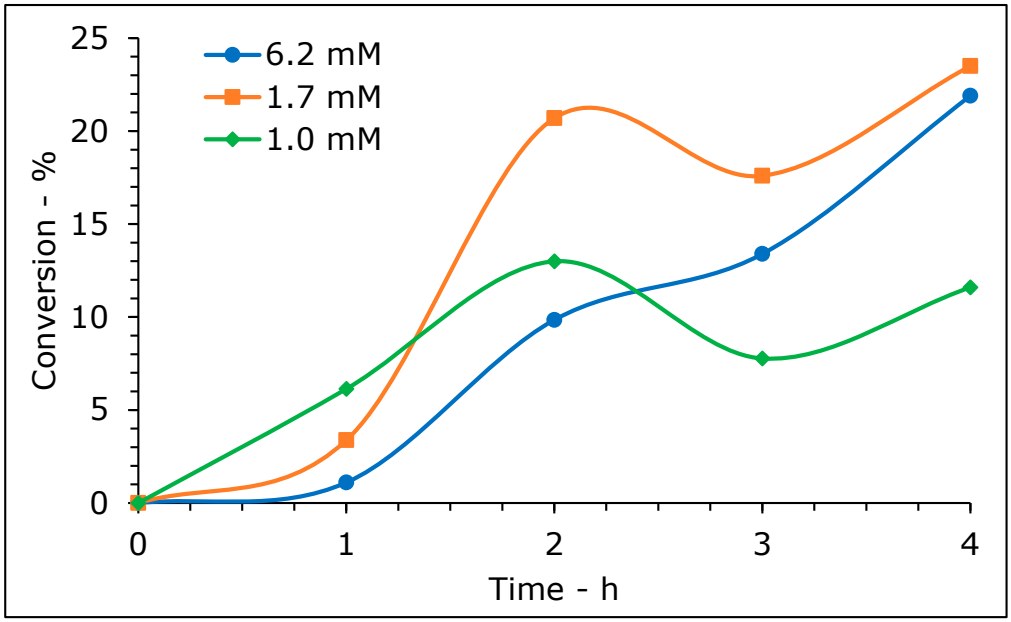

Figure 5. Photo-reduction of NO_3^- under LED lamp with 0.1% Ag/FSP as photocatalyst (0.034 mol_{NO3-}/g_{cat}), various concentration of $NaNO_3$ (1–6.2 mM), pH 5, rt and 1000 mL of solution (Reactor 2).

Although higher concentration of reactant should favour the kinetics, in that case we are working with a photochemical treatment whose yield depends on the total number of irradiated photons, which is fixed, therefore working with lower concentration of substrate molecules causes higher conversion, while keeping the same amount of catalyst (activated equally by the incident photons). By contrast, if the NO_3^- concentration is too low, the reaction kinetics slows down unacceptably, thus, 1.7 mM was selected as the best $NaNO_3$ concentration for the following step, which was the optimisation of the substrate/catalyst ratio. In order to find the best ratio, three tests were performed, with values between 17 and 72 $mmol_{NO3-}/g_{cat}$ (Figure 6). Either increasing or reducing the amount of catalyst caused a drop in nitrate conversion of below 14%. The lower amount of catalyst (72 $mmol_{NO3-}/g_{cat}$) was insufficient and, in fact, an induction time before the beginning of the reaction was observed. On the other hand, higher amounts of titania (17 $mmol_{NO3-}/g_{cat}$) provided more active sites for adsorption and reaction, though it may hinder the passage of the light and determine a loss of activity. Also, in this case the intermediate value showed the highest conversion.

Overall, the interpretation of reaction mechanism and kinetics is not simple, suggesting the role of adsorption or activation phenomena (leading to an induction time), especially in the case of the FSP samples and with an increasing concentration of substrate.

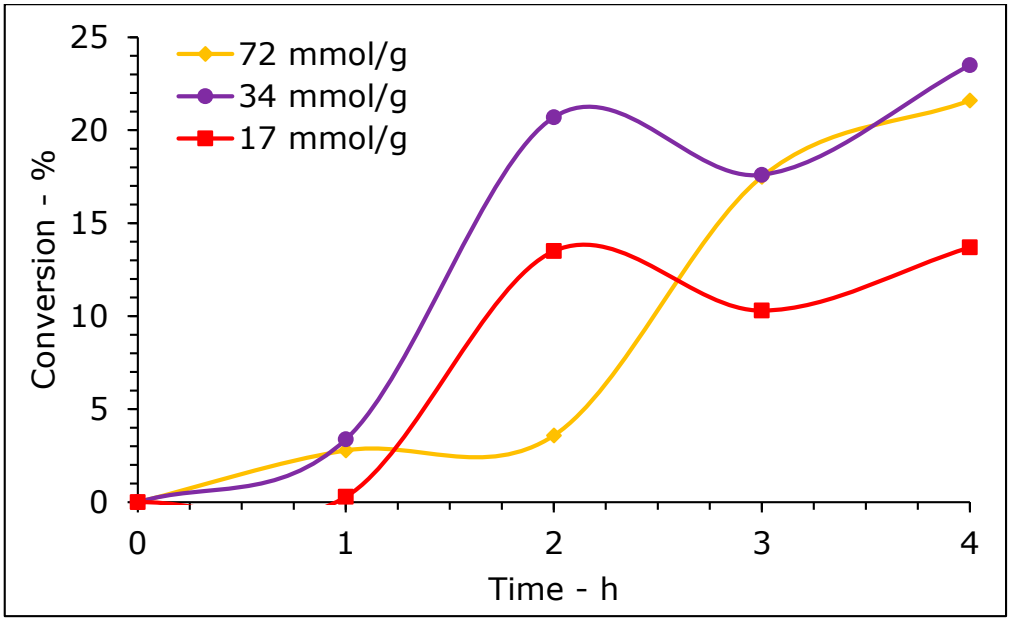

Figure 6. Photo-reduction of NO_3^- under LED lamp using 0.1% Ag/FSP as photocatalyst, with various substrate/cat ratio (17–72 $mmol_{NO3-}/g_{cat}$), $NaNO_3$ (1.7 mM), pH 5, rt and 1000 mL of solution (Reactor 2).

2.4. Comparison of Different Photocatalysts

Once the best conditions in which to perform the reaction were found, a series of metal-deposited catalysts were tested under LED white light irradiation. The results in terms of nitrate conversion are reported in Figure 7a. Despite the expectations, the only catalyst which performed better than the bare P25 is that loaded with silver, resulting in a 23.5% conversion, whereas other materials produced results between 19% (0.1 Au/FPS) and 3% (0.1 Au/P25). In addition, a not negligible selectivity towards ammonium was observed when treating the wastewater with P25 and 1% Ag/P25 (from Figure 7b, ca. 13.5% in both cases), as well as 0.1% Au/FSP, although the latter showed a very little selectivity towards ammonium and nitrite, just in the early stage of the process. Notwithstanding this, a possible explanation for the poor performance achieved with the functionalised catalysts is that the reduction of nitrate is in competition with other reactions, such us the reduction of water to hydrogen. Indeed, this path is kinetically favoured due to the lower number of electrons involved, i.e., 2 vs. 10 for the couple NO_3^-/N_2. Also, as reported by Challagualla et al. [29], the noble metals active in the hydrogen evolution are Pt, Pd due to the favourable position of their sub-bands, which are located below the conduction band (CB), while Ag is more prone to nitrate reduction and releases less hydrogen since its sub-bands are far from CB. Unfortunately, the current photoreactor configuration operates in semi batch mode with He flow and/or open top, preventing the possibility of accumulating significantly and quantifying the possibly evolved H_2.

Ag 1 wt% loading was also found effective for the photoreduction of nitrate in a previous report, due to the effective formation of a Schottky barrier with TiO_2. The presence of co-catalysts and the Ti^{3+}/Ti^{4+} ratio is also reported to affect the selectivity. Ti^{3+} favoured the formation of NH_3, while selectivity to N_2 was shown by the Ti^{4+} sites, both on anatase and rutile facets [30]. Selectivity to N_2 was also higher for Ag-loaded titania with respect to the bare TiO_2 and other co-catalysts (e.g., Au or Cu). Ag is also reported to actively reduce nitrate in $Ag@Bi_4O_5I_2$/SPION@calcium alginate under UV, Visible and NIR irradiation with high selectivity to N_2. The plasmonic-resonance effect is invoked to explain the effect of Ag [31].

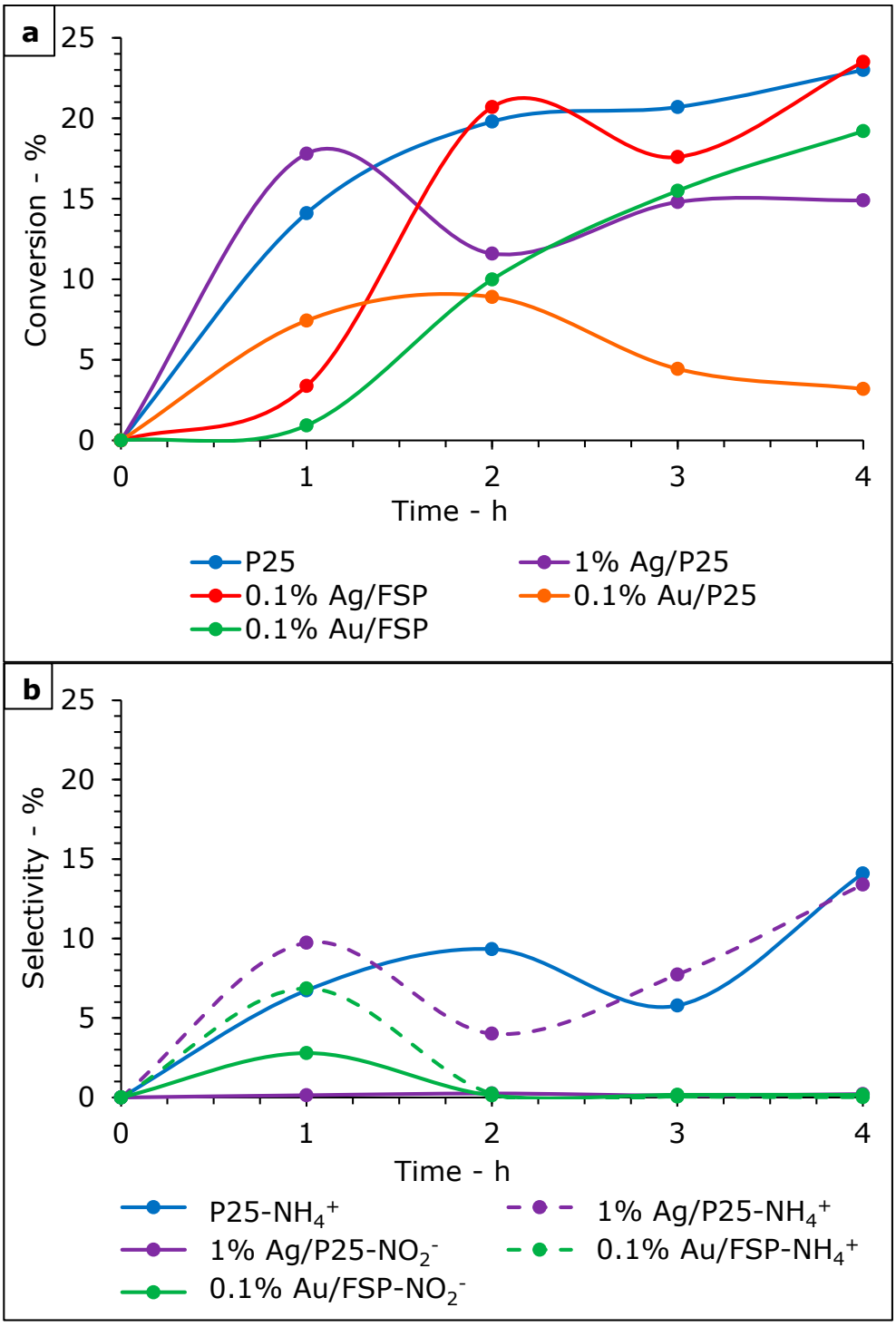

Figure 7. (**a**) Conversion of NO_3^- under LED lamp with several photocatalysts, substrate/cat ratio 34 $mmol_{NO3-}/g_{cat}$, $NaNO_3$ (1.7 mM), pH 5, rt and 1000 mL of solution; (**b**) Selectivity of the photocatalyst towards NH_4^+ and NO_2^-. The amount is negligible if not reported.

The photo-reduction of nitrate was also performed under UV light but using both the best conditions and the more active catalyst found in the case of visible light studies. The following test was conducted with the UV reactor opened to air. Figure 8 shows a slightly better performance over the short period, with a 23.4% conversion of nitrate after 2 h vs. 8.3% of the platinum-deposited catalyst. Moreover, there were no traces of over-reduced compounds or intermediates, such as nitrite. However, a maximum in conversion was

observed which subsequently reached a stable 20% plateau. These results agree with those reported in literature [32], though different studies in the gas phase reduction of NO_x indicated a tight dependence of selectivity to nitrite and nitrate on the radiation intensity, which is not evident here [33]. In addition, silver was preferred for the deposition since it was less expensive than platinum. Moreover, the test was repeated switching to a visible light source and the reaction time was increased to 24 h, which revealed that catalysts based on silver showed a trend similar to what was already observed with 0.1% Pt/FSP. Indeed, there is a maximum conversion of ammonium followed by a plateau for several hours, then the conversion rises again to reach its final value.

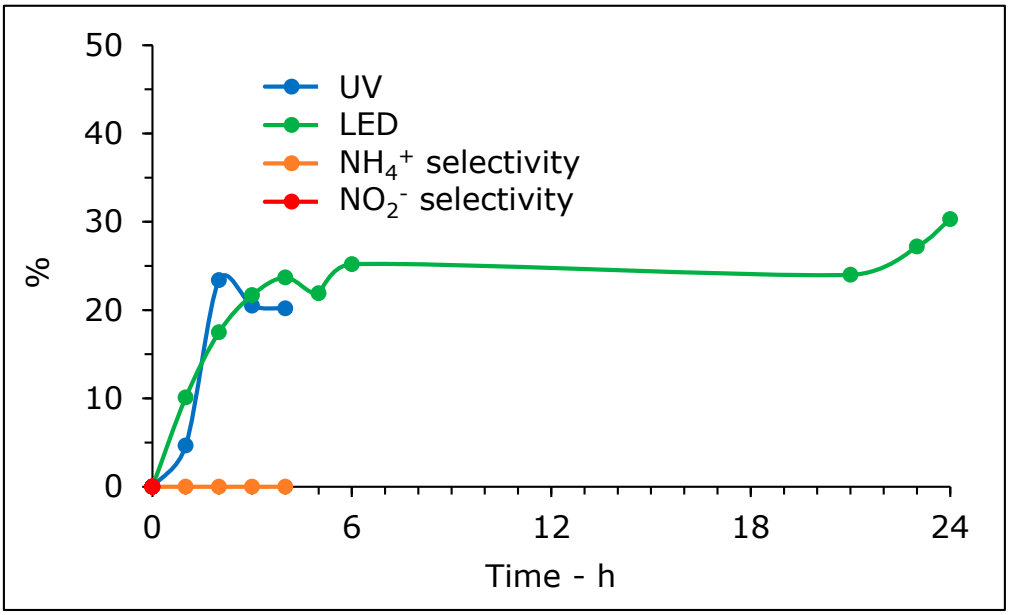

Figure 8. Photo-reduction of NO_3^- under UV lamp (Irr. 260 W/m^2) or LED with 0.1% Ag/FSP as photocatalyst (substrate/cat ratio 34 $mmol_{NO3-}/g_{cat}$), $NaNO_3$ (1 mM), pH 5, rt, 250 mL (UV, Reactor 1) or 1000 mL (LED, Reactor 2) of solution.

To conclude, we attempted to simulate real wastewater by preparation of the nitrate solution with tap water. Figure 9 illustrates that the treatment of a real matrix causes a halving of the catalytic conversion of nitrates, since only 11.3% of the initial amounts of the substrate are mineralized to nitrogen, probably due to the parasitic consumption of electrons by concurring species more prone to be reduced than the nitrate. Even though the process is still under development, and the effect of the real matrix should be much better understood, conversion is still relevant when using tap water, with a similar performance trend. Real application may require increased reactor volume and/or higher power, which may still retain feasible costs, due to relatively inexpensive LED lamps that have very reduced installation costs and consumption.

Furthermore, the purpose of this work was to screen materials and conditions in order to assess the best options for either single photoreduction of nitrates or combined abatement of nitrates and ammonia. The envisaged application is a continuous photoreactor, characterised by sufficiently high irradiance and residence times to achieve the desired conversion/selectivity values, but with immobilised catalysts. Durability tests on such a configuration will be necessary to precisely assess the durability of the assembly.

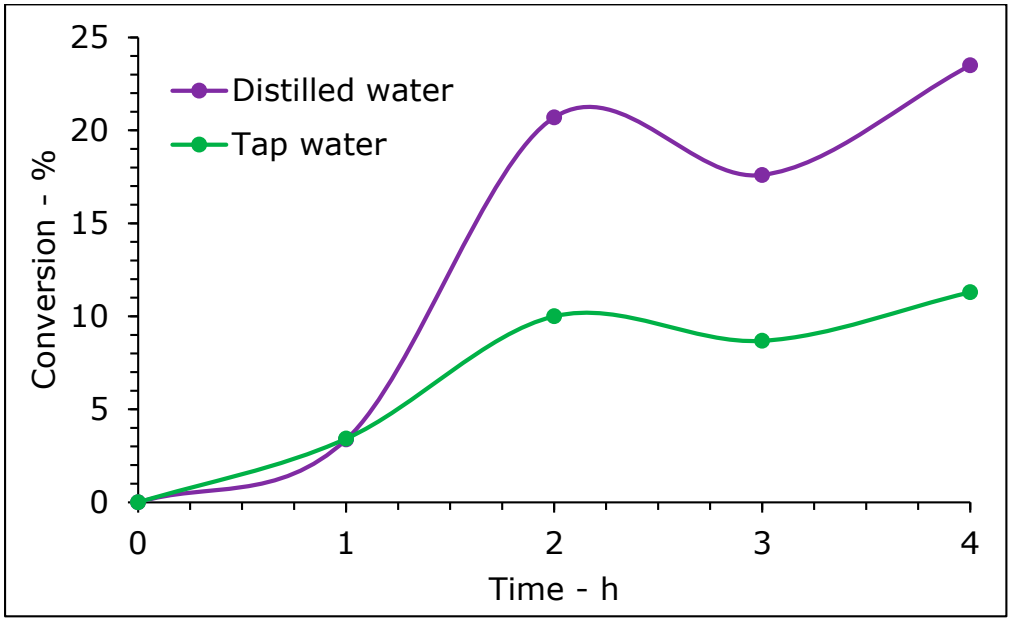

Figure 9. Photo-reduction of NO_3^- under LED lamp using 0.1% Ag/FSP as photocatalyst, substrate/catalyst ratio 34 $mmol_{NO3-}/g_{cat}$, $NaNO_3$ (1.7 mM), pH 5, rt and 1000 mL of solution prepared with distilled or tap water (Reactor 2).

2.5. Combined Photo-Degradation under Visible Light

When a photon of the proper wavelength is absorbed by the photocatalyst, it promotes the formation of a photo-excited electron (e^-) and a hole (h^+). The first is the reducing species which is involved in the photo-reduction of our substrate. However, the hole must be consumed in order to complete the redox reaction. Sometimes, a sacrificial agent (hole scavenger), such as oxalic or formic acid, is added to the reaction mixture since it is easily oxidised by the holes [32,34], preventing a charge accumulation and the fast recombination of the e^--h^+ couple that lowers the efficiency of the photocatalyst. On the contrary, our previous investigation on the use of HCOOH as HS led to the opposite conclusion, with decreasing nitrate conversion at increasing formic acid concentration [35]. Also, in this case, we speculate that the presence of a more effective hole scavenger may favour parallel reactions, such as hydrogen production, which is unfortunately undetectable in the semi-batch configuration of our reactor. Besides this, adding further reactants to treat wastewater is not envisaged, thus an alternative solution is here proposed.

We recently demonstrated that the oxidation of ammonium can occur on the same titania-based catalyst employed so far, and in the same conditions [25,26]; subsequently, a combined photo-treatment was performed to abate, simultaneously, both nitrate and ammonium (Reaction 4).

$$NO_3^- + 1.67\ NH_4^+ \rightarrow 1.83\ N_2 + 3\ H_2O + 0.67\ H^+ \quad (4)$$

The ratio between the reactants was set to the stoichiometric and the degradation was performed in three configurations in order to boost the reactions. The results are reported in Figure 10: firstly, they show that the conversion of both ammonium and nitrate is almost coincident in every stage of the treatment; it is, therefore, probable that both the Redox reactions benefit from each other. The first attempt was made using the LED lamp and a reaction trend quite similar to the expectation was found, with the maximum conversion after around 2 h of irradiation, and a final conversion for both NH_4^+ and NO_3^- of about 20% after 4 h. The nitrate conversion would be rate-limiting in this case, since the literature data for photo-oxidation of ammonia report higher conversion. Overall, it is a promising result since the performance was not worse and the two processes were

carried out simultaneously. Slightly higher conversion, close to 30%, was achieved under UV irradiation, likely taking advantage of the presence of ammonium as a hole scavenger.

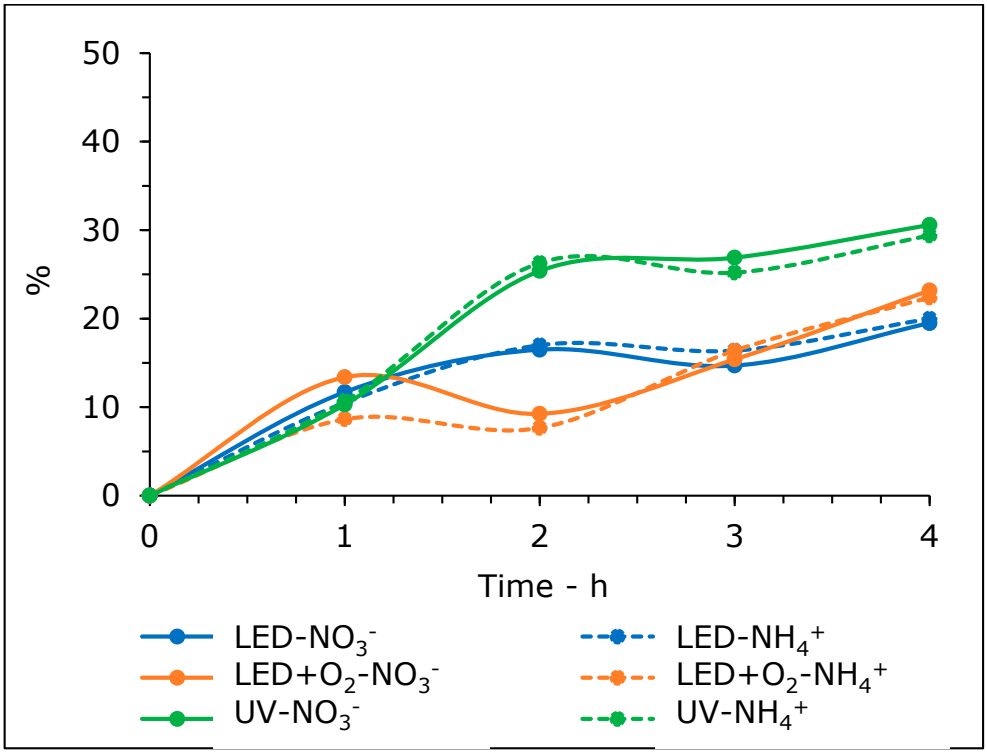

Figure 10. Photo-reduction of NO_3^- under LED or UV lamp using 0.05 g of 0.1% Ag/FSP photocatalyst, $NaNO_3$ (1.7 mM), NH_4Cl (2.8 mM), pH 5, rt and 1000 mL of solution (Reactor 2). LED test was repeated with air bubbling (air flow 12 mL/min).

Lastly, a third test was carried out with a constant air supply flowing through the solution. This setup returned a small increase in the reactor performance in the case of photo-oxidation of ammonium [25]. However, Figure 10 clearly highlights a limited effect of this solution, as the conversion is only pushed up to 22%.

3. Materials and Methods

3.1. Materials Preparation

The photocatalyst P25 is a commercial titania in the form of a nanopowder supplied by Evonik (Essen, Germany) [36]. It is generally constituted of uniform nanoparticles ca. 20 nm in diameter, with a mixed phase of anatase and rutile approximately 70:30. The specific surface area is typically 45–50 m^2/g and the powder is constituted of ca. 20 nm dense nanoparticles.

As a comparison, another flame-based technique, from a different precursor and leading to a different calcination time, and temperature were used. TiO_2 nanoparticles were prepared via flame spray pyrolysis (FSP) using the homemade apparatus previously described in detail [36–38]. Briefly, the apparatus includes a burner with a hole in the centre that is ringed by many flamelets. The latter are fed with a mixture of methane and oxygen (0.5 L/min CH_4 and 1 L/min O_2), while another flow of oxygen (5 L/min) is supplied in the central hole, along with the precursor solution, which is usually prepared dissolving the selected amounts of titanium isopropoxide (Sigma Aldrich − Merck Life Science S.r.l., Milan, Italy, pur. 97%) into xylene + propionic acid (1:1 *v*/*v*). The solution is pumped at a constant rate, for instance 2.7 mL/min, through a needle inserted at the bottom of the burner; it is then dispersed by the oxygen co-current into small drops that are instantly vaporised and burned by the flame. The catalyst, in the form of a nanopowder, is then

deposited over a glass bell which surrounds the burner. The FSP catalysts used in this work were obtained by application of a pressure drop of 1.5 bar at the nozzle.

Metal promotion of the catalysts was achieved through wet impregnation [16], which involves the formation of a clear solution in water by the addition of the selected amount of metal precursor and titania to a round-bottomed flask; the solution is then stirred for 2 h and evaporated under reduced pressure until a homogeneous powder is obtained. Subsequently, the powder is dried in a static oven (105 °C) for one night and reduced in a tubular oven under hydrogen flow (5 °C/min of ramp and 3 h at the maximum reduction temperature indicated in Table 2). The detailed amounts and conditions are reported in Table 2 and were selected after proper TPR analysis.

Table 2. Details for preparation of each catalyst through wet impregnation.

Precursor	Metal to Support Ratio (%mol)	Support	Reduction T (°C)	Appearance
$AgNO_3$ (Sigma Aldrich − Merck Life Science S.r.l., Milan, Italy, >99%)	0.1	TiO_2-FSP	150	Grey-Brown
$AuCl_3$ (Sigma Aldrich − Merck Life Science S.r.l., Milan, Italy, >99%)	0.1	TiO_2-FSP	700	Light Purple
$Pt(acac)_2$ (Sigma Aldrich − Merck Life Science S.r.l., Milan, Italy, >97%)	0.1	TiO_2-P25	700	Grey
$AuCl_3$ (Sigma Aldrich − Merck Life Science S.r.l., Milan, Italy, >99%)	0.1	TiO_2-P25	700	Light purple
$AgNO_3$ (Sigma Aldrich − Merck Life Science S.r.l., Milan, Italy, >99%)	0.1	TiO_2-P25	150	Grey-Brown
$AgNO_3$ (Sigma Aldrich − Merck Life Science S.r.l., Milan, Italy, >99%)	1.0	TiO_2-P25	150	Dark-Grey

3.2. Material Characterisation

Adsorption and desorption isotherms were obtained adsorbing N_2 over the active material at −196 °C after overnight degassing at 150 °C by means of a Micrometrics ASAP2020 apparatus (Norcross, GA, USA).

X-ray diffraction patterns (XRD) were registered on a Rigaku D III-MAX horizontal-scan powder diffractometer (Neu-Isenburg, Germany) equipped with Cu-K Kα radiation and a graphite monochromator on the diffracted beam. Characteristic reflections were assigned by comparison with the standard JCPDS card, 21–1272 for anatase and 21–1276 for rutile. Crystallite size was calculated according to Scherrer equation $\tau = (K\lambda)/(\beta\cos\theta)$, where tau is the mean size of the crystalline domains, K is the shape factor (0.9 was used), beta is the full width at half maximum, expressed in radians, of the peak considered (25.3° for anatase and 27.4° for rutile) and theta is the angle of the reflection.

Diffuse Reflectance (DR) UV-Vis spectra of samples were recorded on a Cary 500 UV-Vis NIR spectrophotometer (Varian instruments, Santa Clara, CA, USA) in the range of 200–800 nm.

Scanning electron microscopy (SEM) was carried out using a FE-SEM LEO 1525 ZEISS (Jena, DE). The scanning electron microscope was equipped with a Bruker Quantax EDX detector. The acceleration potential voltage was maintained at 15 keV and the analyses were done using an AsB detector (Angle selective Backscattered detector) and an In-lens detector. Samples were deposited on conductive carbon adhesive tape and analysed without metallisation.

Transmission Electron Micrographs (TEM) were carried out on a Philips 208 Transmission Electron Microscope (Philips S.p.A., Milan, Italy). The samples were prepared by putting one drop of an ethanol dispersion of the catalysts on a copper grid, pre-coated with a Formvar film and dried in air.

3.3. Procedures and Reactor Setup

Two different photoreactors were used in this work. The first (Reactor 1, Figure 11a) is a cylinder-type round-bottomed reactor with a capacity of about 350 mL and which allows the insertion of a co-axial UV lamp from the top. It can be used in a sealed configuration, for instance to measure the nitrogen evolution, or open to air, as when an external white light LED lamp is employed. The second setup includes a larger reactor (Reactor 2, Figure 11b) with a volume of 3000 mL, which is more suitable for external irradiation, such as UV and LED. The latter is a spotlight-type lamp with a power of 30 W (Yonkers Inspire, 2700 lm, Yonkers, NY, USA) that is fixed over the solution (100 mm). By contrast, the UV lamp employed was a medium pressure-type with one emitting bulb (Jelosil HG 100 AS, Vimercate, Milan, Italy, 125 W, maximum emission at 365 nm) and the irradiance measured with a photoradiometer (delta OHM HD2102.2, Vimercate, Milan, Italy) was ca. 260 W/m^2. External UV lamp irradiance was 116 W/m^2.

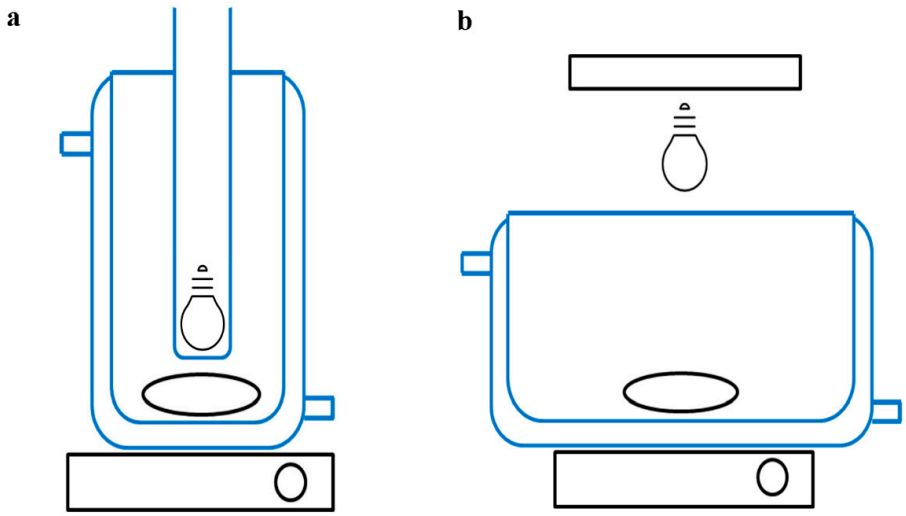

Figure 11. Reactor scheme (**a**) immersed lap (UV) and (**b**) external lamps (UV and LEDs).

All the experiments were carried out selecting the appropriate reactor and adding the selected amount of photocatalyst, sodium nitrate and water. The pH was then adjusted with the minimum amount of diluted hydrochloric acid (0.002 M, from 37% solution). The treatment began when the lamp was switched on.

Nitrogen evolution was monitored qualitatively by connecting the reactor to a gas chromatograph (HP 5890, Santa Clara, CA, USA, Porapak Q + MS columns) and sampling with a 75 mL/min flow of helium.

The liquid phase was sampled with a glass syringe, filtered (cellulose acetate filter, Sartorius Stedim, Goettingen, Germany, 200 nm) in order to remove the solid catalyst and then analysed by means of an ion-exchange chromatograph (Metrohm 883 Basic IC, Metrohm Italiana S.r.l., Origgio (VA), Italy) equipped with an anionic column (Metrosep C 4-250/4,0, Metrohm Italiana S.r.l., Origgio (VA), Italy) in series to a chemical suppressor, which reduces the background noise. The eluent was a water solution of Na_2CO_3 (3.2 mmol/L, 99.5%) and $NaHCO_3$ (1 mmol/L, 99.7%). Moreover, the ammonium possibly formed by over-reduction was analysed with the same instrument after switching to a cationic column (Metrosep A Supp 4-250/4,0, Metrohm Italiana S.r.l., Origgio (VA), Italy) with the proper eluent, which contained HNO_3 (1.7 mmol/L, from 70% solution) and dipicolinic acid (0.7 mmol/L, 99.0%) diluted with HPLC water.

All the chemical reagents were purchased from Sigma Aldrich (Sigma Aldrich–Merck Life Science S.r.l., Milan, Italy) as supplied, without further purification.

The mean error for UV quantification of NH_3/NH_4^+ was <5%, while for IC analysis in the quantification of NO_3^- and NO_2^-, it was <1.5%. Two replicates of each analysis were typically carried out, calculating the average result, except for outliers, where additional tests were added for consistent results.

4. Conclusions

The photo-abatement of nitrate was successfully carried out under both UV and visible light irradiation using titania-based photocatalysts. Firstly, both the irradiation sources employed gave conversions between 30 and 20%, depending on the catalyst. No advantages support the usage of the UV lamp instead of the LED one, since the latter consumes less power (30 W vs. 125 W), releases less heat and lasts longer. Moreover, under visible light, it was found that the most active catalyst was the FSP titania loaded with 0.1% mol of Ag, although it only performed slightly better than bare titania. Other metals with an increase in co-catalyst loading depressed the catalyst performance.

Conversion with 0.1% Ag/FSP fell from 23.5% to 11.3% when using tap water, likely because of multiple species that compete to react with the photogenerated electrons. On the other hand, photo-reduction can be effectively performed in combination with photo-oxidation of ammonium, which is a fully new field of investigation that allows the concomitant abatement of two pollutants.

Author Contributions: Conceptualization, I.R. and G.R.; methodology, F.C.; investigation, V.P. and A.D.M.; resources, I.R. and G.R.; data curation, F.C.; writing—original draft preparation, F.C.; writing—review and editing, I.R. and G.R.; supervision, I.R.; project administration, I.R.; funding acquisition, I.R. All authors have read and agreed to the published version of the manuscript.

Funding: This research was funded by Fondazione Cariplo (Italy), grant number 2015-0186 "DeN—Innovative technologies for the abatement of N-containing pollutants in water". I. Rossetti is grateful to Fondazione Cariplo (Italy) and Regione Lombardia (Italy) for financial support through the grant 2016-0858—"Up-Unconventional Photoreactors". University of Milan is acknowledge to provide funding for publication of this paper as IOAP participant.

Data Availability Statement: All the relevant data are reported in this article.

Conflicts of Interest: The authors declare that they have no conflict of interest.

References

1. Rockström, J.; Steffen, W.; Noone, K.; Persson, Å.; Chapin, F.S.; Lambin, E.F.; Lenton, T.M.; Scheffer, M.; Folke, C.; Schellnhuber, H.J.; et al. A safe operation space for humanity. *Nature* **2009**, *461*, 472–475. [CrossRef] [PubMed]
2. Driscoll, C.T.; Whithall, D.; Aber, J.D.; Boyer, E.; Castro, M.; Cronon, C.; Goodale, C.L.; Groffman, P.M.; Hopkinson, C.; Lambert, K.F.; et al. Nitrogen Pollution: Source and Consequences in the U.S. Northeast. *Environment* **2003**, *45*, 22. [CrossRef]
3. Chislock, M.; Doster, E. Eutrophication: Causes, Consequences, and Controls in Aquatic Ecosystems. *Nat. Educ. Knowl.* **2013**, *4*, 10.
4. Herschy, R.W. *Water Quality for Drinking: WHO Guidelines*; World Health Organization: Geneva, Switzerland, 2012; ISBN 9789241548151.
5. Camargo, J.A.; Alonso, A.; Salamanca, A. Nitrate toxicity to aquatic animals: A review with new data for freshwater invertebrates. *Chemosphere* **2005**, *58*, 1255–1267. [CrossRef] [PubMed]
6. Volkmer, B.G.; Ernst, B.; Simon, J.; Kuefer, R.; Bartsch, G.; Bach, D.; Gschwend, J.E. Influence of nitrate levels in drinking water on urological malignancies: A community-based cohort study. *BJU Int.* **2005**, *95*, 972–976. [CrossRef] [PubMed]
7. Pyatt, F.B. Potential effects on human health of an ammonia rich atmospheric environment in an archaeologically important cave in southeast Asia. *Occup. Environ. Med.* **2003**, *60*, 986–988. [CrossRef]
8. Park, J.Y.; Yoo, Y.J. Biological nitrate removal in industrial wastewater treatment: Which electron donor we can choose. *Appl. Microbiol. Biotechnol.* **2009**, *82*, 415–429. [CrossRef] [PubMed]
9. Nur, T.; Shim, W.G.; Loganathan, P.; Vigneswaran, S.; Kandasamy, J. Nitrate removal using Purolite A520E ion exchange resin: Batch and fixed-bed column adsorption modelling. *Int. J. Environ. Sci. Technol.* **2015**, *12*, 1311–1320. [CrossRef]
10. Ferro, S.; Australia, E. Removal of nitrates from highly-contaminated industrial wastewater Sustainable Environmental Technology for Chemical and Allied industries (SETCA) View project Innovative Technologies for the Remediation of Soils and Waters View project. *La Chim. l'Industria* **2012**, *2*, 100–110.

11. Rek-Lipczynska, A. Purification of the Air in the Historic Cities of Towns. In *IOP Conference Series: Materials Science and Engineering*; IOP Publishing: Bristol, UK, 2019; Volume 471.
12. Fujishima, A.; Rao, T.N.; Tryk, D.A. Titanium dioxide photocatalysis. *J. Photochem. Photobiol. C Photochem. Rev.* **2000**, *471*, 102029. [CrossRef]
13. Parrino, F.; Palmisano, L. (Eds.) *Titanium Dioxide (TiO_2) and Its Applications*; Elsevier Inc.: Amsterdam, The Netherlands, 2021. [CrossRef]
14. Banerjee, S.; Dionysiou, D.D.; Pillai, S.C. Self-cleaning applications of TiO_2 by photo-induced hydrophilicity and photocatalysis. *Appl. Catal. B Environ.* **2015**, *176–177*, 396–428. [CrossRef]
15. Bahadori, E.; Tripodi, A.; Ramis, G.; Rossetti, I. Semi-Batch Photocatalytic Reduction of Nitrates: Role of Process Conditions and Co-Catalysts. *ChemCatChem* **2019**, *11*, 4642–4652. [CrossRef]
16. Bahadori, E.; Tripodi, A.; Villa, A.; Pirola, C.; Prati, L.; Ramis, G.; Dimitratos, N.; Wang, D.; Rossetti, I. High pressure CO_2 photoreduction using Au/TiO_2: Unravelling the effect of co-catalysts and of titania polymorphs. *Catal. Sci. Technol.* **2019**, *9*, 2253–2265. [CrossRef]
17. Anas, M.; Han, D.S.; Mahmoud, K.; Park, H.; Abdel-Wahab, A. Photocatalytic degradation of organic dye using titanium dioxide modified with metal and non-metal deposition. *Mater. Sci. Semicond. Process.* **2015**, *41*, 209–218. [CrossRef]
18. Bahadori, E.; Tripodi, A.; Villa, A.; Pirola, C.; Prati, L.; Ramis, G.; Rossetti, I. High pressure photoreduction of CO_2: Effect of catalyst formulation, hole scavenger addition and operating conditions. *Catalysts* **2018**, *8*, 430. [CrossRef]
19. Kumar, S.G.; Devi, L.G. Review on modified TiO_2 photocatalysis under UV/visible light: Selected results and related mechanisms on interfacial charge carrier transfer dynamics. *J. Phys. Chem. A* **2011**, *115*, 13211–13241. [CrossRef]
20. Yan, H.; Wang, X.; Yao, M.; Yao, X. Band structure design of semiconductors for enhanced photocatalytic activity: The case of TiO_2. *Prog. Nat. Sci. Mater. Int.* **2013**, *23*, 402–407. [CrossRef]
21. Moss, B.; Lim, K.K.; Beltram, A.; Moniz, S.; Tang, J.; Fornasiero, P.; Barnes, P.; Durrant, J.; Kafizas, A. Comparing photoelectrochemical water oxidation, recombination kinetics and charge trapping in the three polymorphs of TiO_2. *Sci. Rep.* **2017**, *7*, 2938. [CrossRef]
22. Hanaor, D.A.H.; Sorrell, C.C. Review of the anatase to rutile phase transformation. *J. Mater. Sci.* **2011**, *46*, 855–874. [CrossRef]
23. Zhang, X.; Cai, M.; Cui, N.; Chen, G.; Zou, G.; Zhou, L. Defective Black TiO_2: Effects of Annealing Atmospheres and Urea Addition on the Properties and Photocatalytic Activities. *Nanomaterials* **2021**, *11*, 2648. [CrossRef]
24. Makuła, P.; Pacia, M.; Macyk, W. How To Correctly Determine the Band Gap Energy of Modified Semiconductor Photocatalysts Based on UV-Vis Spectra. *J. Phys. Chem. Lett.* **2018**, *9*, 6814–6817. [CrossRef] [PubMed]
25. Conte, F.; Pellegatta, V.; Tripodi, A.; Ramis, G.; Rossetti, I. Photo-oxidation of ammonia to molecular nitrogen in water under uv, vis and sunlight irradiation. *Catalysts* **2021**, *11*, 975. [CrossRef]
26. Bahadori, E.; Conte, F.; Tripodi, A.; Ramis, G.; Rossetti, I. Photocatalytic Selective Oxidation of Ammonia in a Semi-Batch Reactor: Unravelling the Effect of Reaction Conditions and Metal Co-Catalysts. *Catalysts* **2021**, *11*, 209. [CrossRef]
27. Silva, C.G.; Pereira, M.F.R.; Órfão, J.J.M.; Faria, J.L.; Soares, O.S.G.P. Catalytic and photocatalytic nitrate reduction over Pd-Cu loaded over hybrid materials of multi-walled carbon nanotubes and TiO_2. *Front. Chem.* **2018**, *6*, 632. [CrossRef]
28. Serpone, N.; Lawless, D.; Disdier, J.; Herrmann, J.-M. *Spectroscopic, Photoconductivity, and Photocatalytic Studies of Ti02 Colloids: Naked and with the Lattice Doped with Cr3+, Fe3+, and V5+ Cations*; American Chemical Societ: Washington, DC, USA, 1994.
29. Challagulla, S.; Tarafder, K.; Ganesan, R.; Roy, S. All that Glitters Is Not Gold: A Probe into Photocatalytic Nitrate Reduction Mechanism over Noble Metal Doped and Undoped TiO_2. *J. Phys. Chem. C* **2017**, *121*, 27406–27416. [CrossRef]
30. Roy, S. Photocatalytic Materials for Reduction of Nitroarenes and Nitrates. *J. Phys. Chem. C* **2020**, *124*, 28345–28358. [CrossRef]
31. Kumar, A.; Rana, A.; Guo, C.; Sharma, G.; M Katubi, K.M.; Alzahrani, F.M.; Naushad, M.; Sillanpää, M.; Dhiman, P.; Stadler, F.J. Acceleration of photo-reduction and oxidation capabilities of $Bi_4O_5I_2$/SPION@calcium alginate by metallic Ag: Wide spectral removal of nitrate and azithromycin. *Chem. Eng. J.* **2021**, *423*, 130173. [CrossRef]
32. Zhang, F.; Jin, R.; Chen, J.; Shao, C.; Gao, W.; Li, L.; Guan, N. High photocatalytic activity and selectivity for nitrogen in nitrate reduction on Ag/TiO_2 catalyst with fine silver clusters. *J. Catal.* **2005**, *232*, 424–431. [CrossRef]
33. Wang, T.; Liu, Y.; Deng, Y.; Cheng, H.; Yang, Y.; Zhang, L. Photochemical reaction of NO_2 on photoactive mineral dust: Mechanism and irradiation intensity dependence. *J. Photochem. Photobiol. A Chem.* **2021**, *416*, 113319. [CrossRef]
34. Adamu, H.; Shand, M.; Taylor, R.S.F.; Manyar, H.G.; Anderson, J.A. Use of carbon-based composites to enhance performance of TiO_2 for the simultaneous removal of nitrates and organics from aqueous environments. *Environ. Sci. Pollut. Res.* **2018**, *25*, 32001–32014. [CrossRef] [PubMed]
35. Bahadori, E.; Compagnoni, M.; Tripodi, A.; Freyria, F.; Armandi, M.; Bonelli, B.; Ramis, G.; Rossetti, I. Photoreduction of nitrates from waste and drinking water. *Mater. Today Proc.* **2018**, *5*, 17404–17413. [CrossRef]
36. P25-EVONIK. Available online: https://corporate.evonik.com/en/products/search-products/pages/product-details.aspx?productId=43469&countryId=5023 (accessed on 22 January 2022).
37. Chiarello, G.L.; Rossetti, I.; Forni, L. Flame-spray pyrolysis preparation of perovskites for methane catalytic combustion. *J. Catal.* **2005**, *236*, 251–261. [CrossRef]
38. Compagnoni, M.; Lasso, J.; Di Michele, A.I.; Rossetti, I. Flame-pyrolysis-prepared catalysts for the steam reforming of ethanol. *Catal. Sci. Technol.* **2016**, *6*, 6247–6256. [CrossRef]